This is the accepted version of the following article: Isarain-Chávez, E. et al. “Micelle-assisted electrodeposition of mesoporous Fe-Pt smooth thin films onto various substrates and their electrocatalytic activity towards hydrogen evolution reaction” in ChemSusChem, vol. 11, issue 2 (Jan.2018), p. 367-375, which has been published in final form at DOI 10.1002/cssc.201701938. **This article may be used for non-commercial purposes in accordance with Wiley Terms and Conditions for Self-Archiving.**

Micelle-assisted electrodeposition of mesoporous Fe-Pt smooth thin films onto various substrates and their electrocatalytic activity towards hydrogen evolution reaction

Eloy Isarain-Chávez, [a] Maria Dolors Baró, [a] Carlos Alcantara, [b] Salvador Pané, [b] Jordi Sort, *[a],[c] and Eva Pellicer **[a]

[a] Dr. E. Isarain-Chávez, Prof. M. D. Baró, Prof. J. Sort, Dr. E. Pellicer Departament de Física Universitat Autònoma de Barcelona E-08193 Bellaterra (Spain) E-mail: Jordi.Sort@uab.cat, Eva.Pellicer@uab.cat
[b] C. Alcantara, Dr. S. Pané Institute of Robotics and Intelligent Systems ETH-Zurich CH-8092 Zurich (Switzerland)
[c] Prof. J. Sort
Institució Catalana de Recerca I Estudis Avançats (ICREA)
Pg. Lluís Companys, 23
E-08010 Barcelona (Spain)
Supporting information for this article is given via a link at the end of the document.

Abstract: Mesoporous Fe-Pt thin films are obtained by micelle-assisted electrodeposition onto metallic substrates with dissimilar activity (namely, gold, copper, and aluminum seed-layers evaporated on Si/Ti) under constant applied potential (E= –1.1 V vs. Ag/AgCl) and deposition time (600 s). The amphiphilic triblock copolymer Pluronic P- 123 is used as a soft-template to guide the formation of mesopores. The occurrence of pores (ca. 7 nm in diameter) with narrow size distribution, regularly distributed over the surface, is observed in all cases. Despite the applied conditions being the same, the roughness and the amount of Fe incorporated in the films are influenced by the substrate nature. In particular, ultra-smooth films containing a larger amount of Fe (21 wt.%) are achieved when deposition takes place on the Au surface. X-ray diffraction analyses reveal that Pt and Fe are alloyed to a certain extent, although some iron oxides/hydroxides also unavoidably form. The resulting films have been tested as electocatalysts in the hydrogen evolution reaction (HER) in alkaline media. The mesoporous Fe-rich Fe-Pt films on Au show excellent HER activity and cyclability.

Introduction

Nanoporous materials are currently in the limelight because of their large surface areas, which make them appealing for many applications including adsorption and separation, catalysis, sensing and fuel cells.[1-4] In the last decade, mesoporous metal oxides, with uniformly sized pores between 2 nm and 50 nm, have been shown to provide enhanced performance in manifold fields.[5] Various chemical synthetic routes, mostly relying on the use of soft and hard templates, can be utilized to grow mesoporous metal oxides in both powder and thin film configurations. [6-9] The conversion of the precursors into the target material is often achieved through a heat treatment process, which is why the production of mesoporous metallic materials is not accessible by this means.[10] Meanwhile, metal mesoporous thin films can be produced by electrodeposition, although their synthesis has proven to be quite challenging. The formation of lyotropic liquid crystal (LLC) phases of amphiphilic molecules in aqueous or ethanolic solutions has been utilized in combination with electrodeposition processes to grow various mesoporous metals on conducting substrates, mostly noble metals such a Pt and Pd and their mixtures,[11-13] and also Co, Ni, Cd, and Sn.[14-17] The main problem of LLC phases (micellar cubic, hexagonal, bicontinuous cubic, lamellar, and inverse micellar) is that the electrolyte turns out to be very viscous, often precluding an efficient stirring of the solutions. The addition of block copolymer surfactants in concentrations above its critical micelle concentration (c.m.c) to guarantee the formation of a micellar solution (L_I) but below the threshold leading to the formation of complex LLC phases is a convenient pathway to produce continuous mesoporous metallic films. Although long-range spatially periodic nanostructures are not easily achievable because the micelles randomly arrange over the substrate, the resulting films feature rather uniformly spaced and sized pores. Recently, the synthesis of mesoporous Pt and Au films using the concept of micelle-assisted electrodeposition has been reported.[18,19]

Mesoporous noble metal (NM)+non-noble metal (NNM) mixtures are interesting for several reasons. First of all, the replacement of costly NMs with more abundant, cheap, non-precious transition metals is in the agenda of current societal challenges.[20] This is of utmost importance, for instance, in electrochemical water splitting processes for hydrogen production. Scientists are continuously seeking how to replace costly Pt by more abundant and cheap elements and/or compounds without compromising the electrocatalytic activity.[21,22] On the other hand, the NNM might bring new functionalities or synergies to the resulting material, making it amenable for different applications. Fe is the fourth most abundant element in the Earth"s crust and it is ferromagnetic. Therefore, it is anticipated that the combination of Pt with Fe can lead to an interesting candidate material for different purposes. Although NM-NM combinations have been already reported in thin film form (e.g. Pt-Au, Pt-Ru),[12,23] the production of NM-NN analogues has been scarcely reported. This is in part due to the dissimilar electrochemical reduction potentials of the NM and NNM salts confined to the aqueous environments of LLC phases. The co-reduction of Pt and Ni species dissolved in the aqueous domain of a LLC phase was demonstrated in the past.[24] In this case, though, powders were obtained in the bulk of the solution since reduction was triggered by the presence of a reducing agent in solution. Yamauchi"s group has made very interesting contributions in the field of mesoporous metallic thin films by electrochemical means. Very recently, a mesoporous Pt-Cu film was prepared by electrochemical micelle assembly[25] and further dealloyed to obtain pure Pt.[26] Ionic liquid-water mixtures have also been described for the preparation of Pt-Co mesoporous films but the

resulting layers were characterized by irregular surfaces according to the scanning electron microscopy (SEM) images.[27] To the best of our knowledge the electrodeposition of mesoporous Pt-Fe films has not been attempted, although Fe-Pt mesoporous nanowires have been recently prepared by selective dealloying.[28] This system is particularly challenging because the inherent complexity of Fe electrochemistry.[29] On the one hand, Fe^{2+} easily oxidizes to Fe^{3+}, which is known to diminish the current efficiency, and on the other hand, oxygen is often included in the deposits in the form of iron oxides/hydroxides. This is why the plating community has been seeking novel formulations to obtain Fe-Pt films with minimized oxygen content.[30]
The nature of the substrate is known to influence the growth of an electrodeposited coating up to several hundreds of nm in thickness.[31] This effect has been often exploited in the manufacture of fully dense metals and alloys to promote a defined texture or grain orientation or to tailor the surface finishing characteristics of the deposited film (e.g. surface roughness).[32] Substrate conditioning is expected to impact even more the morphological characteristics of mesoporous thin films since the asperities of the substrate can modulate to a great extent the nanosized features of these films.
Herein, we describe the synthesis of high-quality, continuous, mesoporous Fe-Pt films by micelle-assisted electrodeposition in aqueous solutions. The surfaces are characterized by being very smooth on gold and copper seed-layers, showing small and evenly distributed pores all over the surface. The triblock copolymer P-123 is used as a structure-directing agent, enabling the discharge of metal salts from the aqueous domains of the electrolyte. The pore walls are crystalline, as demonstrated by X-ray diffraction (XRD) and selected area electron diffraction (SAED) analyses. The seed-layer utilized (namely, gold, copper and aluminum) has a decisive influence on both the topography and the Fe/Pt/O ratio in the films. The latter enables a controllable saturation magnetization. The electrocatalytic activity of the mesoporous thin films towards HER has been evaluated in alkaline media. The results indicate that the film with 21 wt.% Fe shows a remarkable HER activity, being its electrochemical surface area around 7 times larger than its geometrical area.

Results and Discussion

Morphology and composition of the mesoporous Fe-Pt thin films

The electrodeposition of Fe-Pt films was conducted from an optimized aqueous electrolyte containing chloro-complexes of Fe and Pt on three different metallic seed-layers (namely, Au, Cu and Al). The concentration of the P-123 surfactant (5 $g \cdot l_{-1}$) was above the c.m.c. (0.001 wt.% at 35 ºC in water[33]) but far below the concentration at which P-123 forms a cubic gel phase (30 wt.%). At the used concentration, thus, spherical micelles spontaneously form in the electrolyte. Different deposition conditions (bath pH, deposition potential and time) were pre-screened (Figure S1). The selected deposition potential (E = –1.1 V) was shown to yield coherent, mesoporous films on Au, Cu and Al substrates with an appreciable incorporation of Fe. At either lower or higher deposition potentials, the resulting films were either non-mesoporous, discontinuous or did not incorporate Fe (see Figure S1). Also, lower pH values did not work as efficiently (Figure S1). The deposition time was fixed at 600 s in order to secure full coverage of the substrate with a clearly visible, high quality mesostructured film at the SEM. At lower deposition times, the film was too thin to clearly observe any regular mesostructure (Figure S1). The role of P-123 as a structure directing agent was confirmed when electrodeposition was performed in its absence. The resulting films did not feature any evident mesoporosity. Instead, films with a nodular morphology frequently observed in electrodeposited metals and alloys was observed (Figure S2). Figure 1(a,b) shows the FE-SEM images of Fe-Pt films obtained on the Au surface from the P-123 containing electrolyte. The presence of nanometer sized pores all over the film surface was confirmed. The occurrence of narrow cracks was also observed. In spite of these cracks, the films deposited on Au were very flat, especially when compared with those obtained on Al. For the latter, the Fe-Pt films displayed a bumpy or nodular appearance (Figure 1c) but were virtually crack-free. At higher magnification, tiny pores were also observed, although they became a bit ill-defined (Figure 1d). Delamination at the film edges was noticed for Fe-Pt films grown on Al (see Figure S3). The morphology of the film deposited on Cu was halfway between that observed on Au and Al (Figure 4e, 4f) and delamination was not observed. Since films" adhesion was good on both Au and Cu seed-layers but compromised on Al, the formers were subjected to a more profound analysis.
Interestingly, not only the substrate nature had an influence on the topography of the films, but also on their composition. Table 1 lists the Pt, Fe and O contents in the Fe-Pt films obtained on the three substrates. The analysis was made at 5 keV to maximize the response of the deposited film (with a thickness below 1 µm), otherwise the signal coming from the seed-layer was too large and the Fe and Pt signals became mostly undetectable. Therefore, analysis of the data should be done with caution. Remarkably, the amount of oxygen could be kept below 10 wt.% in all films. As a general trend, Fe discharge was favored on Au, whereas its incorporation was lower in the films deposited on Cu and Al. It is thus clear that the activity of the substrate influences the discharge of cations.

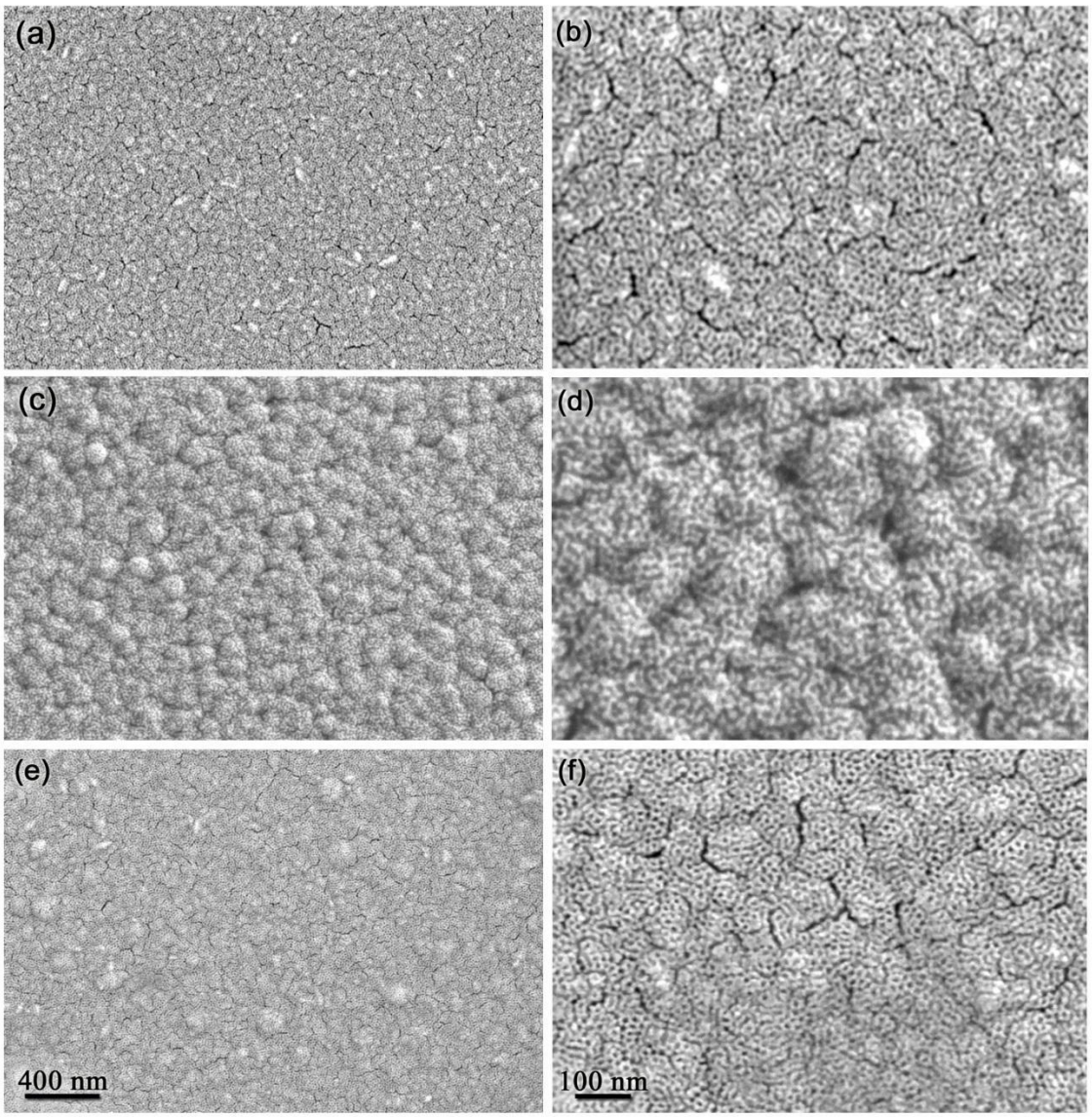

Figure 1. On-top SEM images of mesoporous Fe-Pt films electrodeposited on: (a), (b) Au; (c), (d) Al, and (e), (f) Cu surfaces. The scale bar shown in (e) holds for (a) and (c). Likewise, the scale bar shown in (f) holds for (b) and (d).

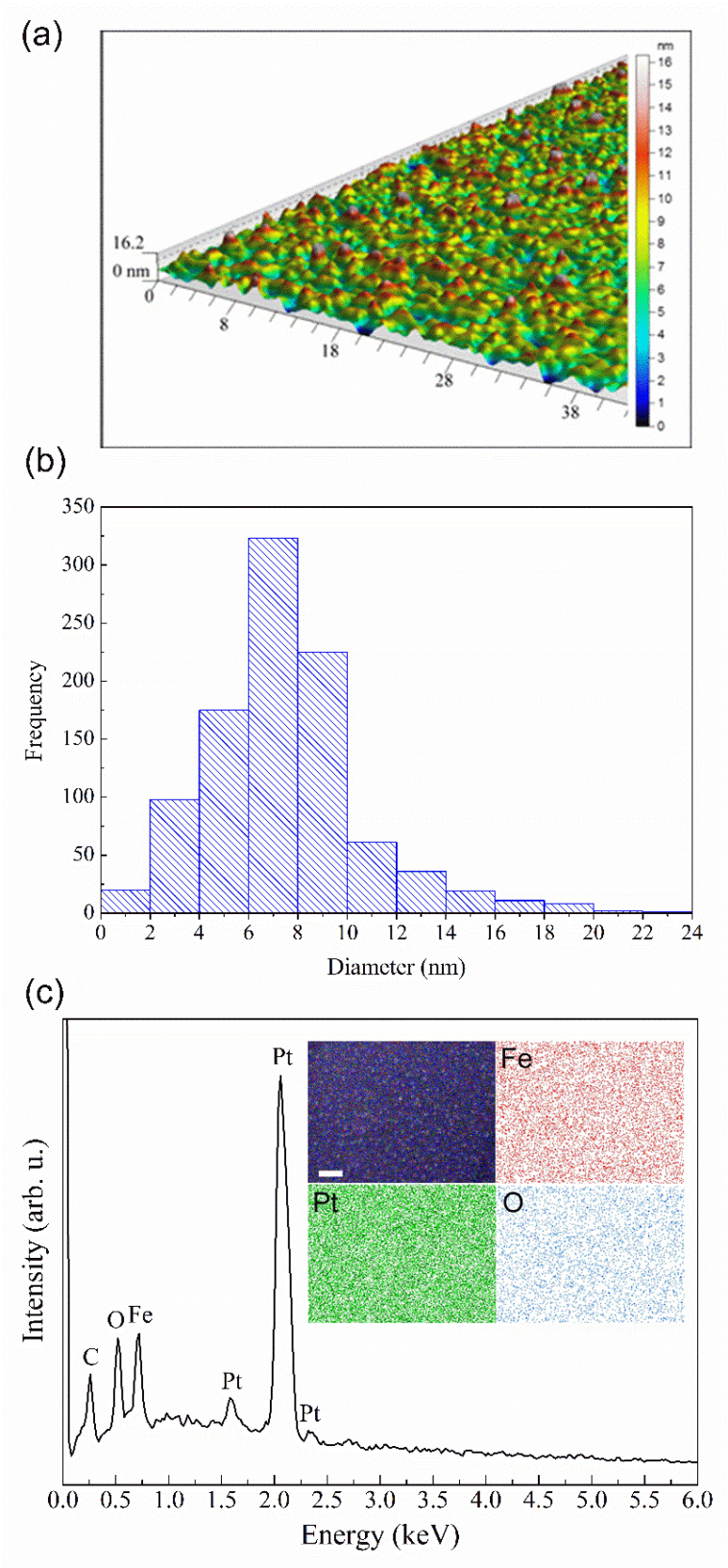

Figure 2. (a) Confocal image of the Fe-Pt film electrodeposited on the Au surface and (b) corresponding histogram of pore size distribution determined from on-top SEM images (see Figure S4). (c) EDX pattern of a film deposited on the Au surface. The inset shows the corresponding EDX mapping. Scale bar in 400 nm.

The Fe/Pt ratio in the films was further confirmed by ICP-OES analyses, showing the same trend as for EDX. Yet, the amount of Fe detected by ICP-OES for the film deposited on Al was higher.

Table 1. Composition of the Fe-Pt films deposited on the various seed-layers, as determined by both EDX and ICP-OES analyses. Note that in EDX the percentages are only indicative since the quantification was done at 5 KeV. The RMS roughness of the mesoporous films is also given.

Electrode surface				**Mesoporous Pt-Fe film**		
Seed-layer	EDX (wt. %)			ICP-OES (wt. %)		RMS (nm)
	Pt	Fe	O	Pt	Fe	
Au	78	17	5	79	21	6.2
Cu	95	3	2	96	4	7.6
Al	89	5	6	86	14	16.3

Figure 2(a) shows the topographic profile obtained by optical profilometry of the Fe-Pt layer deposited on Au. Nanometric, hill-shaped features up to 16 nm are observed on the z-scale. The RMS roughness value of the film was 6.2 nm, indicating its smoothness. Table 1 lists the RMS values of the films deposited on Cu and Al as well. The trend agrees well with the topographical features previously observed by FE-SEM. The corresponding pore size distribution is shown in Figure 2(b). A mean pore size of 7±1 nm was calculated (see Figure 2b). Meanwhile, the pore walls looked slightly thinner. Same results regarding pore size were obtained on Cu.

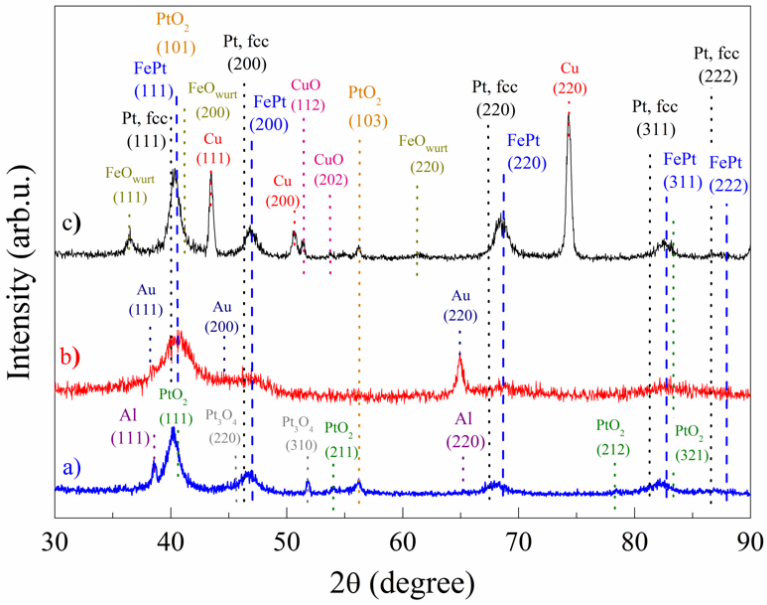

Figure 3. XRD patterns of the Fe-Pt films electrodeposited onto a) Al, b) Au and c) Cu surfaces. The Miller indices of the different phases comprised in the electrodeposited films are indicated. Note that small amounts of two different PtO_2 phases were detected, with space groups P63mc (in orange) and Pnnm (in green).

A representative EDX spectrum of the films is depicted in Figure 2(c), confirming the presence of Fe and Pt elements along with O. The inset is the EDX mapping of the same film, clearly evidencing a homogeneous distribution of the elements across the surface. Finally, the weight amounts of Pt and Fe deposited on each surface is given in Table 2. As aforementioned, the activity of the substrate is an important parameter to take into account. It influences not only the Fe/Pt ratio but also film thickness. The mesoporous Fe-Pt layers deposited on Au and Cu were 100 nm thick (see Figure S5), whereas the films grown on Al were thinner (1/3 of the thickness), which makes sense considering the amount of deposited material.

Table 2. Weight amounts of Fe and Pt electrodeposited on each seed-layer, as determined by ICP-OES.

Electrode surface	**Mesoporous Fe-Pt film**	
Seed-layer	**Fe (□g)**	**Pt (□g)**
Au	7.6	29
Cu	1.3	35
Al	1.7	10

Structural analyses of the mesoporous Fe-Pt thin films

XRD analyses were carried out determine the crystallographic structure of the mesoporous Fe-Pt films. Figure 3 shows the XRD patterns of the films grown on Al, Au and Cu substrates. For the film grown on Cu (Pt-rich film, curve c), the main peaks located at 40º, 46º, 67º and 82º can be ascribed to the face-centered cubic (fcc) phase of Pt. These peaks are slightly shifted toward higher angles with respect to the positions of pure Pt, suggesting the dissolution of some iron in the fcc-Pt cell. Indeed, they are located between the fcc-Pt and the fcc-FePt (50:50) phases. The obtained cell parameter of the fcc- Fe-Pt solid solution grown onto Cu is 0.38819 nm, which is lower than the cell parameter of pure Pt (a = 0.39200 nm). Besides these Fe-Pt alloy peaks, there are several peaks of lower intensity that correspond to the Cu conductive layer, cubic FeO (wurtzite phase, space group Fm-3m), monoclinic CuO (space group C2/c:b1) and oxidized Pt phases. The Miller indices of the diffraction peaks for the different crystallographic phases are indicated in the figure. Interestingly, the width of the fcc-Fe-Pt peaks in the mesoporous film grown onto Au (Figure 3, curve b) is larger, suggesting that the crystallite size is smaller in this case.

Actually, fitting the XRD patterns using the Rietveld method[34,35] gives values of crystallite size around 10 nm for the Fe-Pt film grown onto Cu, 5 nm for the film grown onto Au and 8 nm for the film grown onto Al. Microstrains are of the order of 0.002-0.004 in all cases. Besides the peaks attributed to the Au see-layer, only the reflections ascribed to the Fe-Pt alloy are observed. The main reflections of the Fe-Pt phase are again shifted toward higher angles compared to the positions of pure Pt, even more than for the film grown onto evaporated Cu, indicating that a greater amount of Fe is actually dissolved in the fcc-Pt lattice, reducing the cell parameter even further (a = 0.38777 nm). This makes sense considering that the percentage of Fe detected in the film is higher (21 wt.%).

Complementary TEM analyses of the films were in agreement with XRD results. Figure 4(a) and 4(b) show the HRTEM images of two different regions of the mesoporous Fe-Pt film deposited on the Au surface. The interplanar distance indicated in Figure 4(a) (2.24 Å) matches the (111) plane of fcc-Fe-Pt phase. Meanwhile, the interplanar distance indicated in Figure 4(b) (2.47 Å) matches the (111) plane of FeO wurtzite phase, which is likely present in such small amounts that it could not be detected by XRD (Figure 3, curve a). The diffuse rings of the SAED pattern shown in Figure 4(c) can be assigned to the main Fe-Pt phase.

Magnetic properties

Hysteresis loops of the Fe-Pt mesoporous films deposited onto the three different seed-layers, recorded at room temperature by VSM, are shown in Figure 5. All loops reveal a soft ferromagnetic behaviour with coercivity values, H_C, lower than 50 Oe, in agreement with previous works from the literature on as-deposited (i.e., non-annealed) Fe-Pt alloys.[30,36-38] This behavior is in contrast to the hard-magnetic properties exhibited by the tetragonal ($L1_0$) phase of equiatomic Fe-Pt alloys, typically obtained in thin films by high-temperature sputtering[39] or in electrodeposited films or nanowires after appropriate thermal annealing treatments.[40]
The mesoporous films grown onto Al and Cu exhibit a saturation magnetization value, M_S, lower than 1 emu g^{-1}. This small M_S is due to the low Fe content in these samples (in the range 4 - 14 wt. %, as shown in Table 1). A fraction of Fe gets dissolved into the fcc FePt solid solution and the remaining Fe oxidizes into wurtzite FeO (Figures 3 and 4). A larger M_S is obtained in the film grown onto Au (M_S = 11.8 emu g^{-1}), where the Fe content is also larger (ca. 21 wt.%) and no clear evidence for the formation of wurtzite FeO is observed by XRD (i.e., it is present only in small amounts).
The dependence of M_S on the Fe content for fcc-FePt is seldom reported in the literature. However, M_S was shown to experimentally decrease from ~1000 emu cm^{-3} to ~600 emu cm^{-3} in fcc-FePt sputtered films when the Pt content increased from 54 to 87 wt.%.[41] These values are far below the M_S value for pure bcc-Fe (1700 emu cm^{-3}). Atom-resolved spin polarized density of states calculations for Fe_xPt_{1-x} fcc solid solutions also predict a progressive decrease of magnetization with the Pt content.[42] Hence, the low M_S in the mesoporous FePt films is likely to be related to the formation of the fcc-Fe-Pt solid solution.
The wurtzite FeO phase is known to be antiferromagnetic at room temperature. However, ferromagnetic-like behavior has been reported in antiferromagnetic nanoparticles due to the occurrence of uncompensated spins at the surface.[43] This effect could be exacerbated in the small wurtzite FeO crystals contained in the mesoporous Fe-Pt frameworks, due to the inherently large surface area-to-volume (S/V) ratio of these films. Hence, the presence of wurtzite FeO could also contribute, at least in part, to the observed ferromagnetic-like behavior.

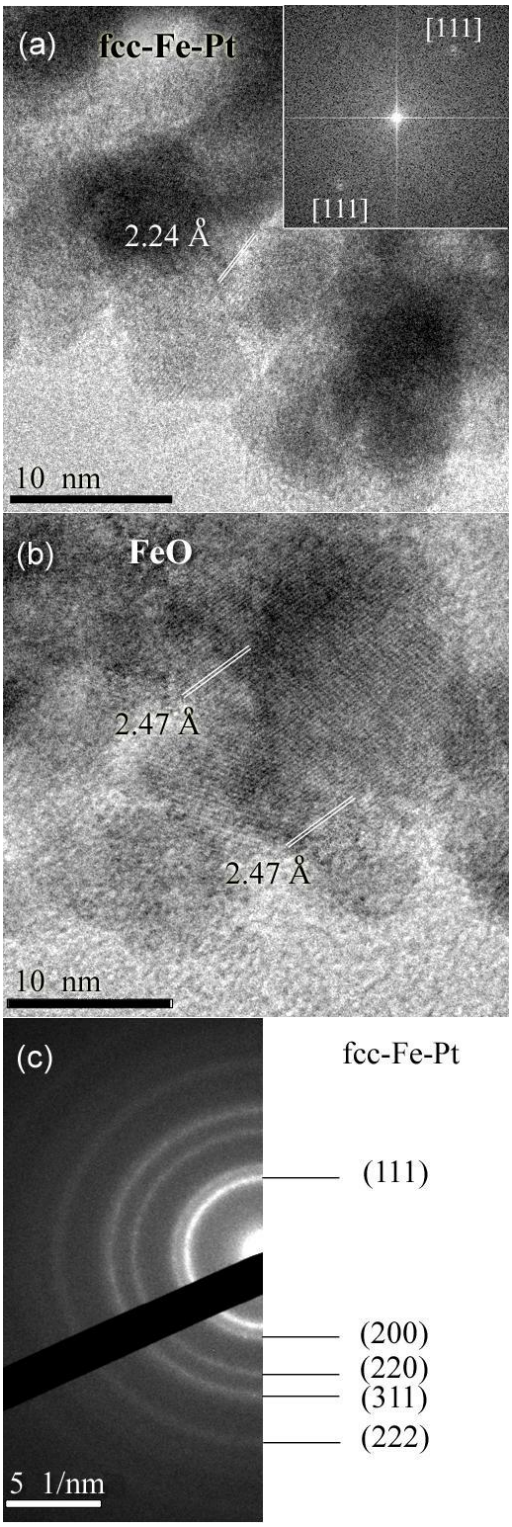

Figure 4. (a,b) HRTEM images corresponding to the mesoporous Fe-Pt film electrodeposited on the Au surface for which a) the indicated interplanar distance and the insert FFT correspond to the fcc-Fe-Pt phase, and b) the interplanar distance corresponds to FeO wurtzite phase. c) SAED pattern showing diffuse rings whose interplanar distances match those of fcc-Fe-Pt phase.

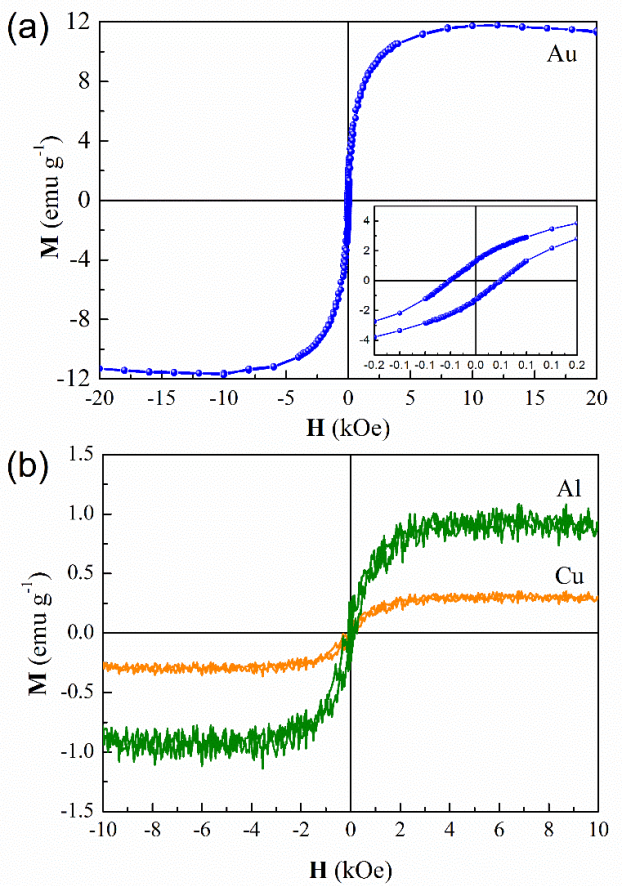

Figure 5. Room-temperature hysteresis loops of the mesoporous Fe-Pt films grown on a) Au, and b) Cu and Al substrates. The inset in (a) shows a detail at low fields.

Electrocatalytic activity towards HER

Figure 6(a) shows the linear sweep voltammetry (LSV) curves (taking the geometrical area into account) recorded in 1 M KOH of the Fe-Pt film deposited on Au. The onset for HER was ca. –7 mV vs. reversible hydrogen electrode (RHE). After 100 cycles, the current density faded slightly. The response of mesoporous pure Pt electrodeposited under analogous conditions (see corresponding SEM image in Fig. S6) was included for comparison purposes. The amount of Pt deposited was similar for both pure Pt and Fe-Pt mesoporous films. A normal criterion is to compare the overpotential vs. RHE at a geometric current density of –10 mA cm^{-2}. Taking this into consideration, the here-designed Fe-rich mesoporous Fe-Pt thin films, characterized by a value of – 74 mV vs. RHE at –10 mA cm^{-2} perform similar to some nanostructured NM-NNM catalyzers reported in the literature.[44,45] The advantage here is the partial replacement of Pt by Fe, one of the most abundant element on the Earth"s crust, which signifies an asset in terms of catalyst"s cost.
In order to have more meaningful values of the current density related to HER, mass-corrected currents for both mesoporous pure Pt and Fe-Pt films grown on Au are given in Figure 6(b)).
The results show that alloying Fe with Pt is indeed beneficial. The specific activity at potentials more negative than –100 mV vs. RHE is higher for the Fe-Pt film than for the electrodeposited pure Pt film.
The electrochemical surface area (ECSA) of the films were determined by the H_{UPD}[46] in 0.5 M H_2SO_4 at –100 mV s^{-1} (Figure 6(c)). The electrodeposited mesoporous pure Pt and Pt-Fe films showed ECSAs of 1.05 cm_2 and 1.85 cm_2, respectively. The corresponding roughness factors, determined as the ratio between the ECSA and the geometric area, are 4.2 and 7.7, respectively. If the mass of electrodeposited Pt is considered, the ECSAs (in m_2 $g_{Pt–1}$) turn out to be 3.2 and 6.4, respectively. Post EDX analyses were performed to confirm that Fe did not dissolve during HER tests. The results indicated that the chemical composition remained the same (see Fig. S7).

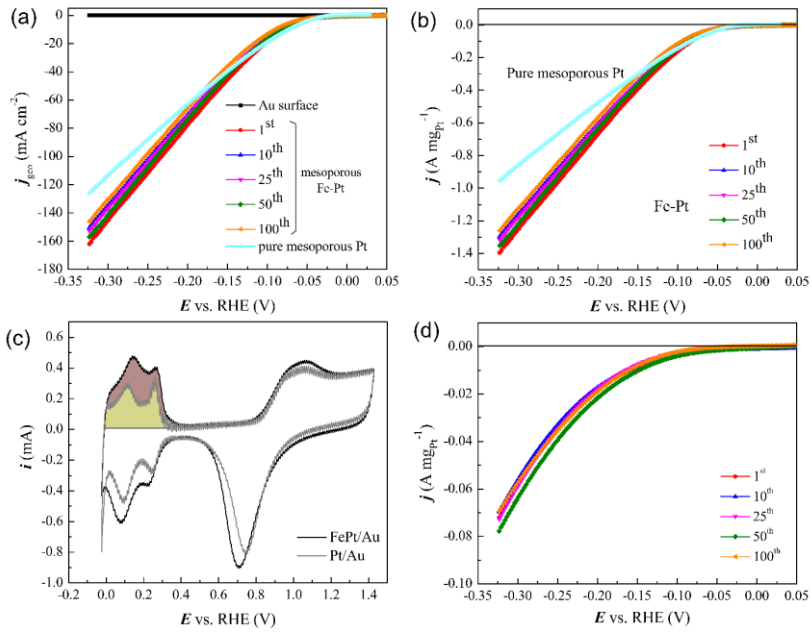

Figure 6. LSV curves recorded in 1M KOH for the Fe-Pt film deposited on the Au surface, for which the current density (*j* = i/A) has been calculated considering (a) the geometrical and b) the mass of deposited Pt (specific activity). c) CV curves recorded for pure Pt and Fe-Pt films deposited on Au in 0.5 M H_2SO_4 at 25 ºC to determine the ECSA values. d) mass-corrected LSV curves recorded in 1M KOH for the Fe-Pt film deposited on the Cu surface

Figure 6(d) shows the LSV curves for the Fe-Pt film deposited on Cu. Although the Pt/Fe ratio is higher compared to the layer grown on Au (see Table 2), their specific activity is 17-fold lower (cf. Figure 6(b) and (d)). In order to shed light on the remarkably lower HER performance of the Fe-Pt film on Cu, XPS analyses were carried out. Figure 7 shows the core-level O 1s, Fe 2p and Pt 4f XPS spectra measured at the outmost surface of the Fe-Pt films deposited on the Au and Cu surfaces. The results indicate that the degree of passivation is higher in the mesoporous film grown on Cu, as could also be envisaged from XRD results (Figure 3). Most importantly, the density of Pt centers exposed to the electrolyte is much higher for the film deposited on Au (Figure 7(c)). The doublet located at 71.0 eV and 74.3 eV corresponds to the $4f_{7/2}$ and $4f_{5/2}$ transitions, respectively, of metallic Pt. Meanwhile, the Fe 2p signal shows a broad, complex band which indicates the presence of some metallic Fe along with iron oxides/hydroxides. The O 1s core-level spectra are also consistent with the higher passivation of the Fe-Pt film formed on Cu. One single peak centered at 530.1 eV assigned to hydroxyl groups is observed for the film deposited on Au. Meanwhile, the O 1s signal of the film grown on Cu can be deconvoluted considering two additional contributions; one located at 532.7 eV attributed to C-OH (and C-O-C) and another one located at 530.6 eV attributed to oxygen linked to metal centers (i.e., Pt-O and Fe- O).[47] The characterization of the Fe-Pt surface after the electrocatalytic tests revealed that the profiles of Fe 2p and O 1s were a bit different than before the tests (Figure S8). Still, the main contribution to the Fe 2p signal around 725 eV attributed to iron oxohydroxide remained.

The mesoporous Fe-Pt films subjected to the HER tests were imaged by FE-SEM and no appreciable damage of the mesostructure was noticed. The high-quality porous network remained intact across the surface and at the film edges (Figure 8). Hence, the here-fabricated mesoporous Fe-Pt layers are good candidates as catalysts for electrochemical water splitting.

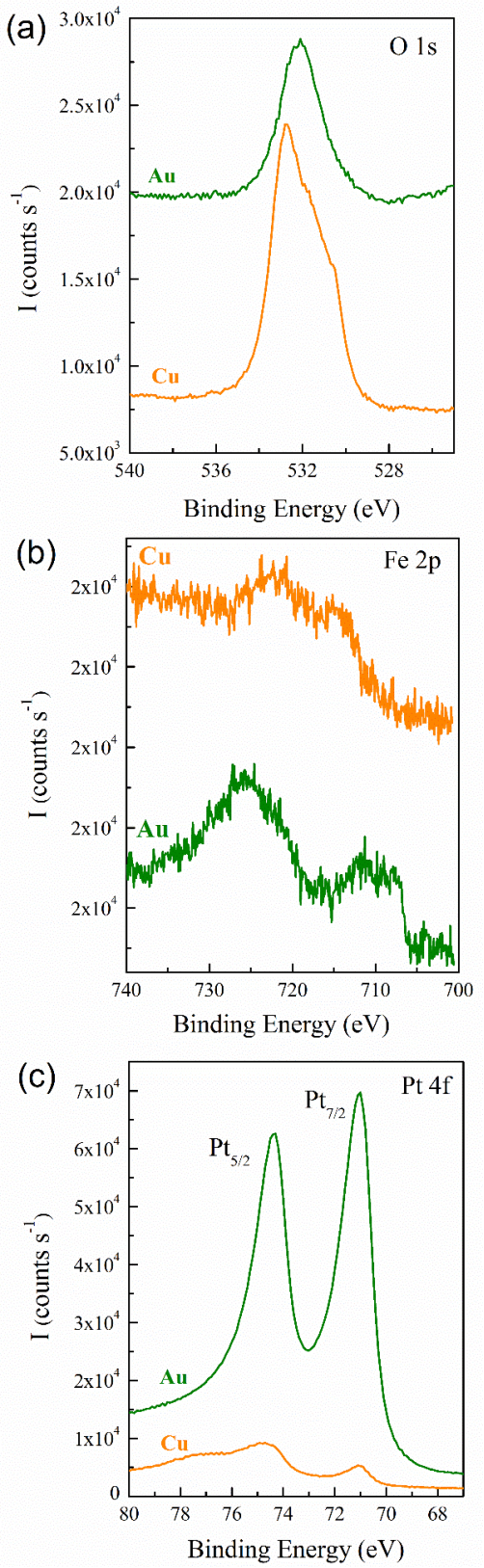

Figure 7. Core-level XPS spectra of (a) O 1s, (b) Fe 2p and (c) Pt 4f for the Fe- Pt films deposited on Au (green curves) and Cu (orange curves).

Conclusions

Fe-Pt mesoporous films with varying Fe/Pt ratios have been electrodeposited on different seed-layers from a tri-block copolymer-containing aqueous bath. Films on Au and Cu seed-layers show very smooth surfaces, whereas those deposited on Al exhibit a hemispherical-like grain morphology, giving rise to higher roughness values. Interestingly, the seed-layer enables certain modulation in the amount of Fe incorporated in the films, that being higher for the case of films deposited on Au. The occurrence of regularly spaced mesopores ca. 7 nm in diameter is observed all over the surface in the three cases. XRD analyses indicate that Fe is mostly reduced to the metallic state, forming a Pt-Fe alloy. The films are bi-functional in the sense that exhibit ferromagnetic properties at room temperature and electrocatalytic activity towards HER in alkaline media. The mesoporous Fe-rich Fe-Pt thin film deposited on Au shows a good HER performance, which can be explained by both its large S/V ratio and the exposure of a large fraction of active Pt centers in contact with the electrolyte. The results herein presented pave the way for the synthesis of functional NM-NNM mixtures in thin film form, with extremely controlled porosity at the nanoscale.

Experimental Section

Electrosynthesis of the Fe-Pt mesoporous films

Mesoporous Fe-Pt films were obtained by micelle-assisted electrodeposition in a triblock copolymer-containing optimized electrolyte. In particular, the electrolyte contained 3.6 mM $FeCl_2 \cdot 4H_2O$, 1.3 mM Na_2PtCl_6, and 5 $g \cdot l_{-1}$ Pluronic P-123 triblock copolymer ($HO(CH_2CH_2O)_{20}(CH_2CH(CH_3)O)_{70}(CH_2CH_2O)_{20}H$). The pH was adjusted to 2.1 by adding 1.0 M HCl. All the solutions were prepared with Millipore Milli-Q water (MQ water-with resistivity > 18 M□ cm at 25 °C). The electrolyte was stable against spontaneous Pt decomposition as no visible colloids formed during the experiments. Also, it did not undergo a color change that could be linked to the oxidation of Fe^{2+} to Fe^{3+}. The electrolyte was stable over 1 month.

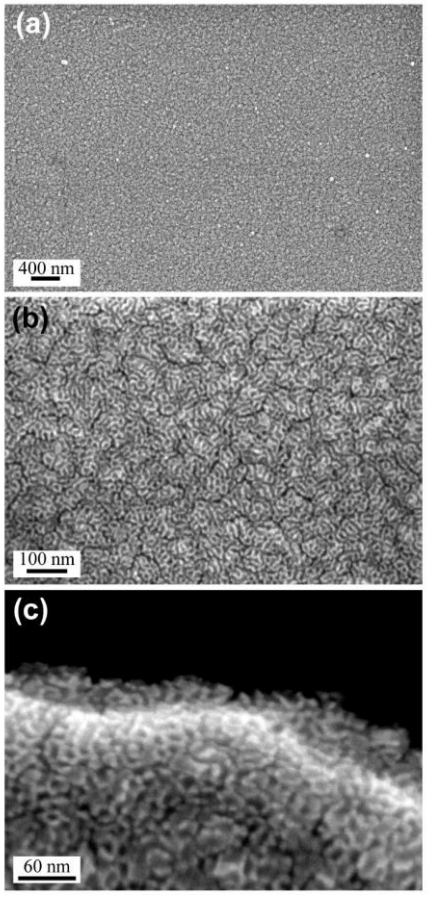

Figure 8. SEM images of the Fe-Pt film deposited on Au after being subjected to 100 LSV cycles in 1 M KOH solution followed by CV tests in 0.5 M H_2SO_4.

Electrochemical deposition was conducted in a double jacketed, three-electrode, single-compartment cell (100 ml) connected to a PGSTAT302N Autolab potentiostat/galvanostat. Si/Ti (25 nm)/*X* (125 nm) (*X*= Au, Cu, Al) substrates of 0.25 cm2 working area were used as the working electrode (WE). A platinum spiral (99.9% purity) was used as a counter electrode (CE), and a double junction Ag|AgCl (*E* = + 0.210 V/SHE) was employed as the reference electrode (RE). The RE contained 3 M KCl as the inner solution and 1 M NaCl as the outer solution. The electrodeposition was

carried out potentiostatically at E = –1.1 V for 600 s under mild stirring (ω = 400 rpm) using a magnetic stirrer bar. The working temperature was 35 ºC. Before each deposition, the bath was de-aerated with N2 gas for 15 min to get rid of oxygen. All substrates were cleaned first with acetone (dipping in it for 20 min), followed by ethanol (10 min), diluted HCl acid (30 s), and rinsed in MQ-water for 3 min. Finally, they were dried with argon gas during 30 s prior to electrodeposition. After electrodeposition, the coated substrates were thoroughly rinsed in acidic water (pH = 2.5) followed by neutral water, and stored under argon to minimize oxidation.

Characterization of the Fe-Pt mesoporous films

Prior to any characterization, the films were further cleaned in UV light (189 nm ≤ □ ≤ 254 nm) for 10 min to fully remove any P-123 traces. When the UV treatment was not applied, the surface of the films looked ill-defined and blurry because of the presence of non-conducting polymer traces covering the film. After UV treatment, it became easier to focus the surface of the films and to get a detail of the features. The corresponding EDX patterns correspondingly show a decrease of the C peak (see Fig. S9). The morphology of the mesoporous Fe-Pt films was examined on a field emission scanning electron microscope (FE-SEM) Zeiss MERLIN operated at 1.2 kV. Energy dispersive X-ray spectroscopy (EDX) analyses were conducted at 5 kV to avoid an exceedingly high penetration into the substrate. Complementary inductively coupled plasma optical emission spectrometry (ICP-OES) analyses were conducted after complete microwave-assisted digestion of the films in aqua regia. Measurements were done on a Perkin Elmer spectrometer Optima 4300DV. Surface roughness and topography were investigated on a Leica DCM 3D dual core 3D optical microscope/profilometer operated in confocal mode with a 100x objective lens. The measurements were made over areas of 150 □m x 100 □m. The crystallographic structure of the mesoporous Fe-Pt films was studied by grazing incidence X-ray diffraction (XRD). Patterns were recorded on a PANalytical X'pert PRO MRD (Materials Research Diffractometer) using Cu Kα radiation (λ = 0.154 nm) at an incidence angle of 1.45°. The patterns were acquired in the 2θ angular range varying from 30° to 90° with a step time of 8 s and a step size of 0.03°. Crystallite sizes, microstrains and cell parameters were estimated from the XRD diffractograms by the full-pattern fitting procedure (Rietveld method) using the MAUD software.[34,35]
High-resolution transmission electron microscopy (HRTEM) observations were conducted on a Jeol-JEM 2011 microscope at 200 kV. Samples for TEM observation were prepared by subjecting the coated substrates to ultrasonication for 20 min in isopropyl alcohol. Afterwards, one or two drops of the resulting suspension were placed dropwise onto a holey carbon-coated Cu TEM grid. X-ray photoelectron spectroscopy (XPS) analyses were done on a PHI 5500 Multitechnique System (Physical Electronics) spectrometer, equipped with a monochromatic X-ray source (Al K□ radiation energy = 1486.6 eV at an applied power of 350 W). The analyzed region was 0.8 mm and the films were placed perpendicular to the analyzer axis, calibrated using 3d5/2 line of Ag with a full width at half maximum (FWHM) of 0.8 eV. Charging effects were corrected by referencing the binding energies of the adventitious C1s line at 284.5 eV. The room-temperature magnetic properties of the mesoporous Fe-Pt films were measured with a vibrating sample magnetometer (VSM) (MicroSense, LOT Quantum Design). The hysteresis loops were recorded along the parallel-to-plane direction with a maximum applied magnetic field of 20 kOe.
The electrocatalytic activity of the films towards hydrogen evolution reaction (HER) was studied in the same three-electrode cell used for deposition, at 25 ºC in 1 M KOH. In this case, the Fe-Pt films grown onto Si/Ti/Au and Si/Ti/Cu substrates were used as the WE. The potentials were converted to RHE for the ease of comparison. The experiments were done on a PGSTAT204 Autolab potentiostat/galvanostat (Metrohm- Autolab) run with NOVA 2.0 software. The electrolyte was purged with Ar gas for 10 min before each experiment. The films were electrochemically pre-treated by running 10 cycles from −0.19 to −0.60 vs. RHE at 50 mV s−1. After that, linear sweep voltammetry (LSV) curves were recorded between 0.05 and −0.32 V vs. RHE at a scan rate of 50 mV s−1. 100 cycles were run to assess materials" stability. ECSAs of the catalysts were determined by the Hupd method, cycling the potential in 0.5 M H2SO4 at a scan rate of 100 mV s−1. The ECSAs of the catalysts were calculated using the equation ECSA=*Q*/(*q*0 x gPt), in which *Q* is the electric quantity calculated from hydrogen desorption peaks, and *q*0 is 210 μC cm−2.

Acknowledgements

Financial support by the European Research Council (SPIN-PORICS 2014-Consolidator Grant, Agreement No. 648454), the Spanish Government (MAT2017-86357-C3-1-R, MAT2014- 57960-C3-1-R and associated FEDER), the Generalitat de Catalunya (2014-SGR-1015) and the L"Oréal-Unesco „For Women in Science" (9th Spanish Edition) and „International Rising Talents" 2015 programmes (awarded to E.P.) is acknowledged. E.I.-C. (Consejo Nacional de Ciencia y Tecnología, in Mexico, CONACYT) for his postdoctoral grant (274347) and E.P. is grateful to MINECO for the “Ramon y Cajal” contract (RYC-2012- 10839). C.A. and S.P. acknowledge financial support by the Marie Skłodowska-Curie Innovative Training Network (H2020- MSCA-ITN-2014) under grant agreement 642642 (SELECTA). The authors would also like to acknowledge networking support by the COST Action e-MINDS MP1407.

Keywords: hydrogen evolution reaction • mesoporous alloy film • iron • platinum • micelle-assisted electrodeposition

[1] G. Sneddon, A. Greenaway and H. H. P. Yiu, *Adv. Energy Mater.* **2014**, *4*, 1301873.
[2] L. Wang and F.-S. Xiao, *Green Chem.* **2015**, *17*, 24–39.
[3] A. Prim, E. Pellicer, E. Rossinyol, F. Peiró, A. Cornet and J. R. Morante, *Adv. Funct. Mater.* **2007**, *17*, 2957–2963.
[4] J. Tang, J. Liu, N. L. Torad and T. Kimura, *Nano Today* **2014**, *9*, 305– 323.
[5] Y. Ren, Z. Ma and P. G. Bruce, *Chem. Soc. Rev.* **2012**, *41*, 4909– 4927.
[6] X. Deng, K. Chen and H. Tüysüz, *Chem. Mater.* **2017**, *29*, 40−52.
[7] C. Park, J. Jung, C. W. Lee and J. Cho, *Sci. Rep.* **2016**, 39136.
[8] T. Brezesinski, J. Wang, S. H. Tolbert and B. Dunn, *Nature Mater.* **2010**, *9*, 146–151.
[9] J. Fan, M. Guerrero, A. Carretero-Genevrier, M. D. Baró, S. Suriñach, E. Pellicer and J. Sort, *J. Mater. Chem. C*, **2017**, *5*, 5517–5527.
[10] J. Zhang and C. M. Li, *Chem. Soc. Rev.* **2012**, *41*, 7016–7031.

[11] G. S. Attard, P. N. Bartlett, N. R. B. Coleman, J. M. Elloitt, J. R. Owen and J. H. Wang, *Science* **1997**, *278*, 838–840.

[12] Y. Yamauchi, A. Tonegawa, M. Komatsu, H. Wang, L. Wang, Y. Nemoto, N. Suzuki and K. Kuroda, *J. Am. Chem. Soc.* **2012**, *134*, 5100−5109.

[13] H. Wang, S. Ishihara, K. Ariga and Y. Yamauchi, *J. Am. Chem. Soc.* **2012**, *134*, 10819−10821.

[14] H. Luo, L. Sun, Y. Lu and Y. Yan, *Langmuir* **2004**, *20*, 10218–10222.

[15] P. A. Nelson, J. M. Elliott, G. S. Attard and J. R. Owen, *Chem. Mater.* **2002**, *14*, 524–529.

[16] F. Bender, R. K. Mankelow, D. B. Hibbert and J. J. Gooding, *Electroanal*. **2006**, *18*, 1558–1563.

[17] A. H. Whitehead, J. M. Elliott, J. R. Owen and G. S. Attard, *Chem. Commun.* **1999**, 331.

[18] H. Wang, L. Wang, T. Sato, Y. Sakamoto, S. Tominaka, K. Miyasaka, N. Miyamoto, Y. Nemoto, O. Terasaki and Y. Yamauchi, *Chem. Mater.* **2012**, *24*, 1591–1598.

[19] C. Li, Ö. Dag, T. D. Dao, T. Nagao, Y. Sakamoto, T. Kimura, O. Terasaki and Y. Yamauchi, *Nature Commun.* **2015**, *6*, 6608.

[20] R. Morris Bullock (Ed.), Catalysis without precious metals, Wiley- VCH, September **2010**.

[21] P. Wang, K. Jiang, G. Wang, J. Yao and X. Huang, *Angew. Chemie* **2016**, *55*, 12859–12863.

[22] J. Zhang, M. D. Baró, E. Pellicer and J. Sort, *Nanoscale* **2014**, *6*, 12490–12499.

[23] H. Wang, M. Imura, Y. Nemoto, L. Wang, H. Young Jeong, T. Yokoshima, O. Terasaki and Y. Yamauchi, *Chem. Eur. J.* **2012**, *18*, 13142.

[24] Y. Yamauchi, S. S. Nair, T. Momma, T. Ohsuna, T. Osaka and K. Kuroda, *J. Mater. Chem.* **2006**, *16*, 2229–2234.

[25] C. Li and Y. Yamauchi, *Chem. Eur. J.* **2014**, *20*, 729–733.

[26] C. Li, V. Malgras, A. Aldalbahi and Y. Yamauchi, *Chem. Asian J.* **2015**, *10*, 316–320.

[27] A. Serrà, E. Gómez, I. V. Golosovsky, J. Nogués and E. Vallés, *J. Mater. Chem. A* **2016**, *4*, 7805–7814.

[28] J.-I. Shui, C. Chen, J. C. M. Li, *Adv. Funct. Mater.* **2011**, *21*, 3357−3362.

[29] J. J. Mallett, E. B. Svedberg, S. Sayan, A. J. Shapiro, L. Wielunski, T. E. Madey, W. F. Egelhoff and T. P. Moffat, *Electrochem. Solid-State Lett.* **2004**, *7*, C121–C124.

[30] D. Liang, J. J. Mallett and G. Zangari, *ACS Appl. Mater. Interfaces*, **2010**, *2*, 961–964.

[31] L. Guo, G. Oskam, A. Radisic, P. M. Hoffmann and P. C. Searson, *J. Phys. D Appl. Phys.* **2011**, *44*, 443001.

[32] I. Tabakovic, J. Gong, S. Riemer and M. Kautzky, *J. Electrochem. Soc.* **201**5, *162*, D102–108.

[33] G. Wanka, H. Hoffmann and W. Ulbricht, *Macromolecules* **1994**, *27*, 4145.

[34] L. Lutterotti and P. Scardi, *J. Appl. Cryst*. **1990**, *23*, 246–252.

[35] MAUD (Materials Analysis Using Diffraction), http://maud.radiographema.com/.

[36] H. L. Nguyen, L. E. M. Howard, G. W. Stinton, S. R. Giblin, B. K. Tanner, I. Terry, A. K. Hughes, I. M. Ross, A. Serres and J. S. O. Evans, *Chem. Mater.* **2006**, *18*, 6414–6424.

[37] K. Leistner, J. Thomas, H. Schlörb, M. Weisheit, L. Schultz and S. Fähler, *Appl. Phys. Lett.* **2004**, *85*, 3498–3500.

[38] S. Thongmee, J. Ding, J. Y. Lin, D. J. Blackwood, J. B. Yi and J. H. Yin, *J. Appl. Phy*s. **2007**, *101*, 09K519.

[39] Z. L. Zhao, J. S. Chen, J. Ding, J. B. Yi, B. H. Liu and J. P. Wang, *Appl. Phys. Lett.* **2006**, *88*, 052503.

[40] L. Cagnon, Y. Dahmae, J. Voiron, S. Pairis, M. Bacia, L. Ortega, N. Benbrahim and A. Kadri, *J. Magn. Magn. Mater.* **2007**, *310*, 2428– 2430.

[41] C.-M. Kuo, P. C. Kuo and H.-C. Wu, *J. Appl. Phys*. **1999**, *85*, 2264– 2269.

[42] P. Vlaic and E. Burzo, *J. Optoelectron. Adv. Mater.* **2010**, *12*, 1114– 1124.

[43] S. A. Makhoulf, F. T. Parker, F. E. Spada and A. E. Berkowitz, *J. Appl. Phys.* **1997**, *81*, 5561.

[44] Z. Cao, Q. Chen, J. Zhang, H. Li, Y. Jiang, S. Shen, G. Fu, B. Lu, Z. Xie and L. Zhen, *Nature Commun*. **2017**, *8*, 15131.

[45] X. Qian, T. Hang, S. Shanmugan and M. Li, *ACS Appl. Mater. Interfaces* **2015**, *7*, 15716–15725.

[46] W. Sheng, H. A. Gasteiger and Y. Shao-Horn, *J. Electrochem. Soc.* **2010**, *157*, B1529–B1536.

[47] K. R. Rasmi, S. C. Vanithakumari, R. P. George, C. Mallika and U. Kamachi Mudali, *RSC Advances* **2015**, *5*, 108050–108057.